Rev.Adv.Mater.Sci. 18(2008) 71-76

GLASS FORMING ABILITY OF $(Cu_{50}Zr_{50})_{96}M_4$ (M=NONE, Al, Nb) BULK METALLIC GLASSES

Tanya Aycan Baser and Marcello Baricco

Dipartimento di Chimica IFM and NIS, Università di Torino, Via P.Giuria, 9 – 10125 Torino, Italy

Received: March 29, 2008

Abstract. The effect of minor addition of Al and Nb on bulk glass formability in $Cu_{50}Zr_{50}$ alloy is investigated. Quenching rate effect was followed comparing the results obtained on ribbons and on different sections of cone-shaped ingots. The phase mixture has been clarified for each alloy, combining structural, microstructural and composition analyses. A fully amorphous phase has been found in ribbons, whereas only for $(Cu_{50}Zr_{50})_{96}Al_4$ a bulk metallic glasses has been obtained. Minor Al addition hinders the formation of the CuZr martensite phase. The effect of composition on the glass forming abilty has been evaluated with emprical parameters, but only the calculation of driving forces for nucleation of crystal phases, using the CALPHAD method, may explain the results.

1. INTRODUCTION

Recent progress on bulk glass formation in binary alloys has triggered interest in easy glass forming systems [1]. Suitable minor alloying addition is very effective for improving the glass forming ability (GFA) of binary alloys [2], such as in the case of Al addition to Cu-Zr binary system [3]. It has also been reported that minor Nb addition enhances the glass forming ability of Cu-Zr system [4]. The improvement of glass forming ability is related to the suppression of nucleation of intermetallic phases [5].

It has been suggested that, for bulk metallic glasses, as the Poisson ratio decreases, the material becomes more brittle [6,7]. Since both elemental Al and Nb have a Poisson ratio higher than Cu and Zr, minor additions of Al and Nb in Cu-Zr system should improve the plasticity of the binary system.

In this paper, the effect of Al and Nb on GFA in $(Cu_{50}Zr_{50})_{96}M_4$ (M=none, Al, Nb) alloys is reported. In particular, the effect of the quenching rate on phase selection is investigated. The positive effect of addition of 4% of Al on glass formation in $Cu_{50}Zr_{50}$ has been explained on the basis of driving forces for nucleation of crystal phases, calculated by CALPHAD method.

2. EXPERIMENTAL

Master alloys ($Cu_{50}Zr_{50}$, $Cu_{48}Zr_{48}Al_4$, and $Cu_{48}Zr_{48}Nb_4$) have been prepared from pure elements by arc melting under Ar atmosphere. Each ingot was remelted several times in order to obtain a good homogeneity. Melt spinning technique was used to obtain ribbons. The liquid alloy was cast in a cone-shaped copper mould in Ar atmosphere and slices of 2 mm, 4 mm, and 6 mm in diameter were obtained from the as-cast ingots. In order to estimate the variation of quenching rate on various slices of the cone-shaped samples, experimental data of temperature versus time obtaiend during quenching Mg-based alloy have been considered [8]. From the analysis of the raw data, for positions where the sample thickness is 3 mm and 6.5 mm in a wedge-shaped mold it turns out that, as the diameter doubles, cooling rate decreases to half. So, a linear correlation between slice diameter and

Corresponding author: Marcello Baricco, e-mail: marcello.baricco@unito.it

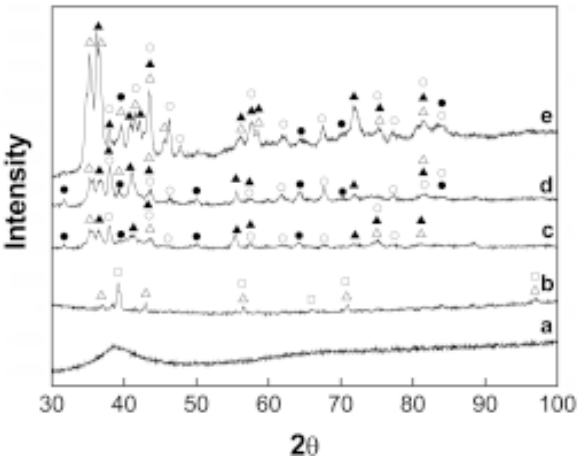

Fig. 1. XRD patterns of $Cu_{50}Zr_{50}$ alloy: ribbon (a), slices of as-cast sample with diameter of 2 mm slice (b), 4 mm (c), 6 mm (d) and master alloy (e). Symbols correspond to $Cu_{10}Zr_7$ (O), CuZr martensite, basic structure (Δ), CuZr martensite, super structure (▲), CuZr cubic (□) and $CuZr_2$ (●) phases.

quenching rate can be considered for a cone-shaped mold. X-ray diffraction (XRD) (Cu K_α) was performed to examine the structure. The microstructure was studied using optical microscope and composition analysis was carried out with EDS. Thermal analysis was performed by differential scanning calorimetry (DSC) at heating rate of 10 °C/min.

3. RESULTS AND DISCUSSION

The effect of the quenching rate on the glass formation in $Cu_{50}Zr_{50}$ alloy was studied by XRD and the results are reported in Fig. 1. The XRD pattern of the master alloy can be fully indexed with $Cu_{10}Zr_7$, $CuZr_2$ and CuZr martensic phase [9,10]. In fact, high temperature CuZr cubic phase might undergo a martensitic transformation on cooling below 140 °C [11]. According to the phase identification, there is no equilibrium of phases even in the master alloy. The same phase mixture was observed in the slices of the as-cast sample with diameter of 6 mm and 4 mm, whereas only CuZr cubic and CuZr martensitic phases were observed in the 2 mm slice. The optical micrograph of the $Cu_{50}Zr_{50}$ master alloy is shown in Fig. 2a. EDS analysis showed that phase I is enriched in Zr (55 at.%), whereas an enrichment in Cu is observed in phase II (64 at.%). So, these phases have been assigned to $CuZr_2$ and $Cu_{10}Zr_7$, respectively. The needle shaped phase III might be associated to the CuZr martensite. The microstructures observed in the 6 mm, 4 mm, and 2 mm slices of the as-cast sample are shown Figs. 2b, 2c, and 2d, respectively. As the ingot diameter decreased, because of the increased quenching rate, the grain size decreased and the microstructure is refined.

XRD results obtained on $(Cu_{50}Zr_{50})_{96}Al_4$ system are shown in Fig. 3. The pattern of the master alloy can be fully indexed considering CuZr cubic, $Cu_{10}Zr_7$, $CuZr_2$ and AlCuZr crystalline phases. CuZr cubic, $Cu_{10}Zr_7$ and AlCuZr phases were also observed in the 6 mm and 4 mm slices of the as-cast sample, whereas only the $Cu_{10}Zr_7$ phase embedded in an amorphous matrix was observed in the 2 mm slice of the ingot. Phase identification shows that minor Al addition to $Cu_{50}Zr_{50}$ hinders the formation of CuZr martensite, suggesting that $Cu_{10}Zr_7$ is the first nucleating phase on cooling. The microstructure of the $(Cu_{50}Zr_{50})_{96}Al_4$ master alloy is shown in Fig. 4a. EDS analysis showed that only phase I contains Al, so phase I, II and III have been assigned to AlCuZr, $CuZr_2$, and $Cu_{10}Zr_7$ crystal structures, respectively. Finer microstructures have been observed in 6 mm slice (Fig. 4b) and 4 mm slice (Fig. 4c), whereas no crystals have been observed in the 2 mm slice of the as-cast sample.

XRD patterns of $(Cu_{50}Zr_{50})_{96}Nb_4$ samples are reported in Fig. 5. CuZr martensite and unknown phases have been observed in the master alloy, as well as in the 6 mm and 4 mm slices of the as-cast sample. In the XRD pattern of slice with 2 mm diameter, main contributions from CuZr cubic phase were found, together with additional diffraction peaks due to the martensite phase, without evidence of an amorphous phase.

A fully amorphous phase has been obtained by rapid solidification for all compositions (Figs. 1, 3, and 5). The DSC traces of crystallization of the amorphous ribbons and of the $(Cu_{50}Zr_{50})_{96}Al_4$ bulk samples are shown in Fig. 6. Glass transition (T_g) and crystallization (T_x) temperatures and heat of crystallisation (ΔH_x) are summarised in Table 1. The melting (T_m) and liquidus (T_l) temperatures and the heat of melting (ΔH_m) for various compositions have been determined by high temperature DSC and the results are collected in Table 1. Al addition to $Cu_{50}Zr_{50}$ amorphous alloy increases the cystallisation temperature, whereas Nb addition decreases it. As the diameter of the bulk samples increased, the intensity of the crystallization event decreased, because of the reduced amorphous

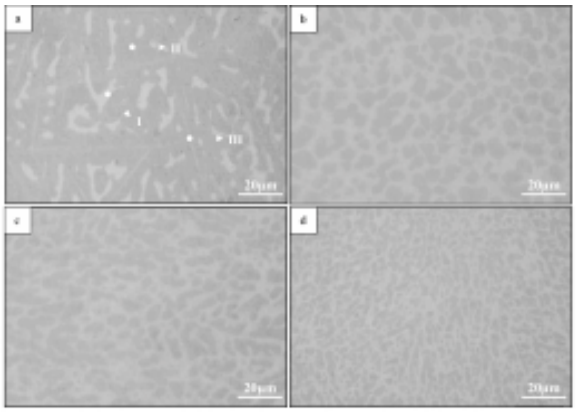

Fig. 2. Optical micrographs for: $Cu_{50}Zr_{50}$ master alloy (a), slices of as-cast sample with diameter of 6 mm (b) 4 mm (c) and 2 mm (d).

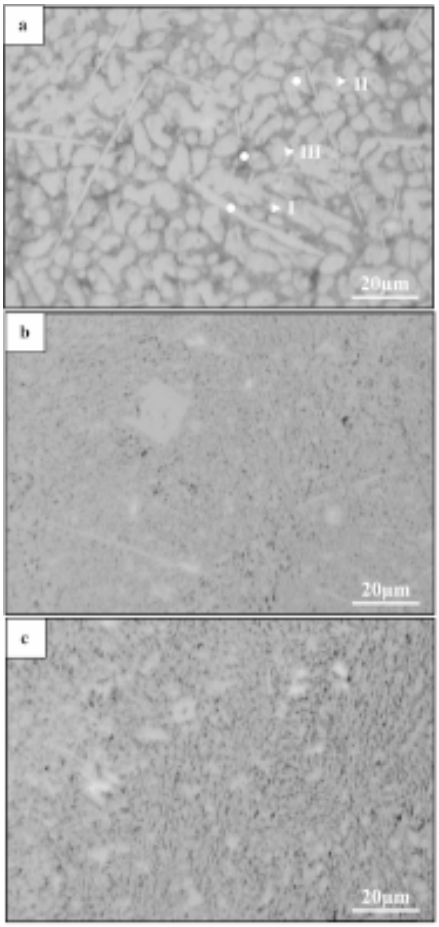

Fig. 4. Optical micrograph for: $(Cu_{50}Zr_{50})_{96}Al_4$ master alloy (a), slices of as-cast sample with diameter of 6 mm (b) and 4 mm (c).

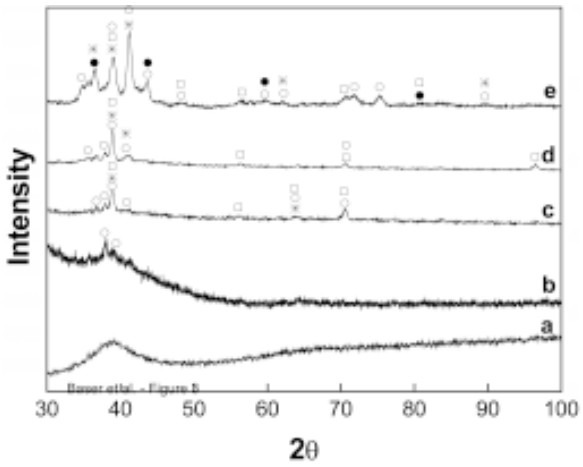

Fig. 3. XRD patterns of $(Cu_{50}Zr_{50})_{96}Al_4$ alloy: ribbon (a), slices of as-cast sample with diameter of 2 mm slice (b), 4 mm (c), 6 mm (d) and master alloy (e). Symbols correspond to $Cu_{10}Zr_7$ (O), $CuZr_2$ (●), CuZr cubic (□), and AlCuZr (*) phases.

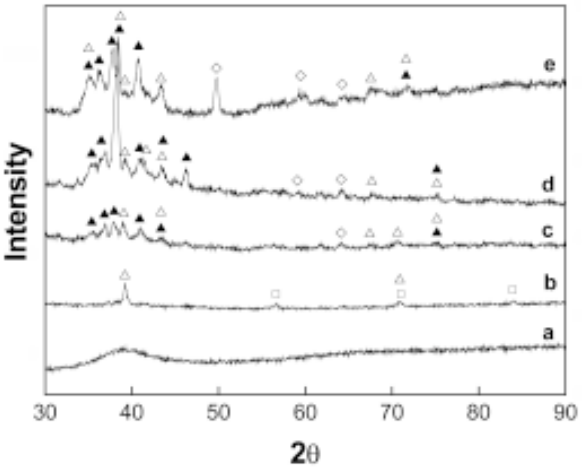

Fig. 5. XRD patterns of $(Cu_{50}Zr_{50})_{96}Nb_4$ alloy: ribbon (a), slices of as-cast sample with diameter of 2 mm slice (b), 4 mm (c), 6 mm (d) and master alloy (e). Symbols correspond to CuZr martensite, basic structure (△), CuZr martensite, super structure (▲), CuZr cubic (□), and unknown (◊) phases.

fraction due to the decreased quenching rate (Table 1).

The GFA of alloys may be defined on the basis of empirical parameters [12], such as $\Delta T=T_x-T_g$, $T_{rg}=T_g/T_l$ and $\gamma= T_x/(T_g+T_l)$. The addition of 4% Al and Nb to $Cu_{50}Zr_{50}$ does not affect significantly the supercooled liquid region (ΔT), but a slight enhancement of T_{rg} and γ was obtained for $(Cu_{50}Zr_{50})_{96}Al_4$ alloy with respect to $Cu_{50}Zr_{50}$ and $(Cu_{50}Zr_{50})_{96}Nb_4$ (Table 1). In this case, empirical parameter cannot fully explain the significant increase of GFA due to the Al addition to $Cu_{50}Zr_{50}$,

Table 1. Thermal data obtained from DSC traces: T_m=melting temperature, T_l=liquidus temperature, ΔH_m=enthaphy of fusion, T_g=glass transition temperature, T_x= crystallisation temperature, $\Delta T=T_x-T_g$, ΔH_x= enthalpy of crystallisation.

Composition	T_m[a] (°C)	T_l[a] (°C)	ΔH_m[a] (J g^{-1})	T_g (°C)	T_x (°C)	ΔT (°C)	ΔH_x (J g^{-1})	Amorphicity (%)	T_{rg} (T_g/T_l)[b]	γ ($T_x/(T_g+T_l)$)[b]
$Cu_{50}Zr_{50}$ (ribbon)	878	940	97	421	471	50	52	100	0.57	0.39
$(Cu_{50}Zr_{50})_{96}Nb_4$ (ribbon)	860	926	94	416	466	50	54	100	0.58	0.39
$(Cu_{50}Zr_{50})_{96}Al_4$ (ribbon)	866	915	84	425	476	51	53	100	0.59	0.40
$(Cu_{50}Zr_{50})_{96}Al_4$ (2 mm)				425	473	48	52	98	0.59	0.40
$(Cu_{50}Zr_{50})_{96}Al_4$ (4 mm)				424	476	52	48	90	0.59	0.40
$(Cu_{50}Zr_{50})_{96}Al_4$ (6 mm)				424	474	50	36	68	0.59	0.40

[a]Data obtained from master alloys.
[b]T_{rg} and γ were defined in Ref [12].

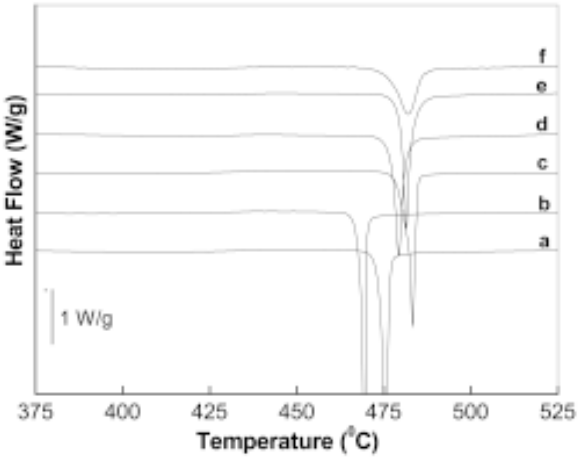

Fig. 6. DSC traces for the crystallisation of $Cu_{50}Zr_{50}$ ribbon (a), $(Cu_{50}Zr_{50})_{96}Nb_4$ ribbon (b), $(Cu_{50}Zr_{50})_{96}Al_4$ ribbon (c), $(Cu_{50}Zr_{50})_{96}Al_4$ as-cast sample taken from the slices with diameter of 2 mm (d), 4 mm (e) and 6 mm (f) .

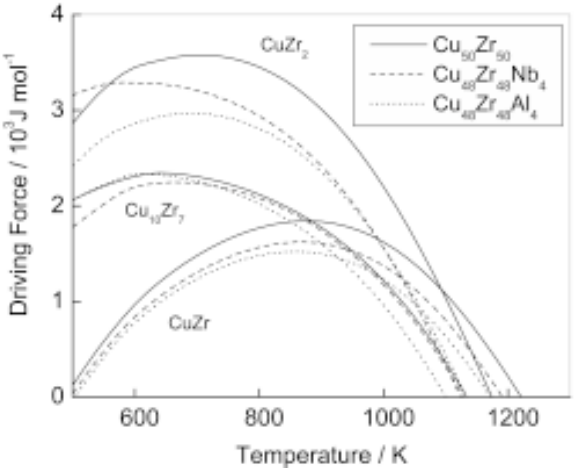

Fig. 7. Driving force for nucleation of crystal phases as a function of temperature, calculated according to the CALPHAD method.

so a thermodynamic analysis of GFA has been carried out by the CALPHAD method [13].

The driving force for nucleation of a crystal phase form the undercooled liquid can be easily estimated if a description of the free energy of both phases is available as a function of temperature and composition. For ternary systems, a thermodynamic description can be obtained by interpolation of the assessed binaries. In order to understand the role of thermodynamics on glass formation in the investigated systems, a recently as-

sessed Cu-Zr phase diagram [14] has been considered as a base system. In this case, a specific thermodynamic description for the undercooled liquid and amorphous phases has been introduced, in order to take into account experimental values of glass transition. In order to obtain information on the effect of the addition of 4% of Al and Nb to $Cu_{50}Zr_{50}$ on the driving force for nucleation of crystalline Cu-Zr phases, the assessed Al-Cu [15], Al-Zr [16], Cu-Nb [17] and Nb-Zr [18] systems have been selected. The results of the calculated driving forces for nucleation of CuZr cubic, $CuZr_2$, and $Cu_{10}Zr_7$ crystal phases from the undercooled liquid are reported in Fig. 7 as a function of the temperature. Because of the lack of data on the thermodynamic description of CuZr martensite and of ternary phases, only Cu-Zr equilibrium crystal phases have been considered. As a consequence of the thermodynamic description of the undercooled liquid, which includes an excess heat capacity, the driving force increases on undercooling, reaches a maximum and then decreases for lower temperatures. For all phases, the highest driving force is obtained for a liquid alloy with composition $Cu_{50}Zr_{50}$. During the quenching of the liquid alloy, CuZr cubic is the first phase showing a tendency to nucleate, but $CuZr_2$ shows the highest driving force for nucleation for an high degree of undercooling. The addition of 4% of Nb and Al to $Cu_{50}Zr_{50}$ reduces the driving force for nucleation, but this effect appears more important for Al addition. Even if the phase selection might be modified for kinetic reasons, the thermodynamic analysis of driving forces for nucleation of crystal phases may explain the observed increase of GFA due to the Al addition to $Cu_{50}Zr_{50}$.

4. CONCLUSIONS

The effect of minor additions of Al and Nb on glass-forming ability of $Cu_{50}Zr_{50}$ has been investigated. The effect of the quenching rate on bulk glass formation has been followed considering ribbons and sliced samples with different diameters, taken from a cone-shaped as-cast ingot. All ribbons were amorphous. Fully crystalline bulk samples have been obtained for $Cu_{50}Zr_{50}$ and $(Cu_{50}Zr_{50})_{96}Nb_4$. For $(Cu_{50}Zr_{50})_{96}Al_4$, samples with increasing diameter showed decreasing amorphous fraction, because of the reduced quenching rate. Thermal data have been collected from DSC measurements. Empirical GFA parameters cannot explain the increase in GFA due to the addition of Al to $Cu_{50}Zr_{50}$. So, the driving forces for nucleation of crystal phases have been calculated by the CALPHAD method, showing that Al addition leads to a decrease of them with respect to the binary system.

ACKNOWLEDGEMENTS

This work was performed for Regione Piemonte, Nanomat, COFIN/MIUR 2005-097983_002 and MCRTN-CT-2003-504692.

REFERENCES

[1] J. Das, M. B. Tang, K. B. Kim, R. Theissmann, F. Baier, W. H. Wang and J. Eckert // *Phys. Rev. Lett.* **94** (2005) 205501.

[2] W. H. Wang, Q. Wei and H. Y. Bai // *Appl. Phys. Lett.* **71** (1997) 58.

[3] W. H. Wang, J. J. Lewondowski and A. L. Greer // *J. Mater Res.* **20** (2005) 2307.

[4] J. Xia, J. Qiang, Y. Wang, Q. Wang and C. Dong // *Appl. Phys. Lett.* **88** (2006) 101907.

[5] P. Yu, H. Y. Bai, M. B. Tang and W. L. Wang // *J. Non-Crys. Solids* **351** (2005) 1328.

[6] Y. Zhang and A. L. Greer // *J. All. and Comp.* **434–435** (2007) 2.

[7] J. Eckert, J. Das, K. B. Kim, F. Baier, M.B. Tang, W.H. Wang and Z.F. Zhang // *Intermetallics* **14** (2006) 876.

[8] N. H. Pryds, M. Eldrup, M. Ohnuma, A. S. Pedersen, J. Hattel and S. Linderoth // *Mater. Trans. JIM* **41** (2000) 1435.

[9] D. Schryvers, G. S. Firstov, J. W. Seo, J. Van Humbeeck and Y. N. Koval // *Scripta Mater.* **27** (1997) 1119.

[10] Z. Y. Liu, M. Aindow, J. A. Hriljac and I. P. Jones // *J. Metastable and Nanocryst. Mater.* **223** (2001) 360.

[11] Y. N. Koval, G. S. Firstov and A. V. Kotko // *Scripta Metall. Mater.* **27** (1992) 1611.

[12] D. Xu, G. Duan and W. L. Johnson // *Phys. Rev. Lett.* **92** (2004) 245504.

[13] M. Palumbo, G. Cacciamani, E. Bosco and M. Baricco // *Calphad* **25** (2001) 625.

[14] T. Abe, M. Shimono, M. Ode and H. Onodera // *Acta Mater.* **54** (2006) 909.

[15] N. Saunders, *Al-Cu system*, In: I. Ansara, A. T. Dinsdale, M. H. Rand, *COST 507: Thermochemical Database for Light Metal Alloys* (European Communities, Luxemburg, 1998), p. 28.

[16] N. Saunders // *Z. Metallk.de* **80** (1989) 894.
[17] C. Michaelsen, C. Gentle and R. Bormann // *J. Appl. Phys.* **81** (1997) 6024.
[18] A. F. Guillermet // *Z. Metallk.de* **82** (1991) 478.